Journal of Engineering Physics and Thermophysics, Vol. 80, No. 1, 2007

APPLICATION OF A TWO-LAYER MODEL OF TURBULENCE IN CALCULATION OF A BOUNDARY LAYER WITH A PRESSURE GRADIENT

K. N. Volkov

UDC 532.529:536.24

The characteristic features of the formulation of a two-layer turbulence model and its application in calculation of near-wall turbulent flows are considered. Factors that influence the effectiveness of implementation of the model and ways of expanding the limits of its applicability are discussed. The possibilities of the two-layer model are demonstrated by calculating a boundary layer on a flat plate with a longitudinal pressure gradient. A comparison of the results of calculation of the heat-transfer characteristics by the two-layer model, two-parameter dissipation model, and Spalart–Allmaras model with the data of a physical experiment and available correlations is made.

Introduction. Despite the intense development of computational techniques and the advances made in the field of constructing numerical methods and the corresponding development of software, the problem of numerical simulation of turbulence remains a most complex one in fluid mechanics.

In engineering applications, wide use is made of the mathematical models based on numerical solution of Reynolds-averaged Navier–Stokes (RANS) equations. Problems on closing Reynolds equations are solved at different levels of complexity [1, 2]. Usually, turbulence models are classified by the number of differential equations introduced additionally to the initial system of equations of motion and heat transfer. Models involving one equation (one-parameter models or first-order models) describe turbulence with the aid of one variable, for which the equation of transfer is constructed; other characteristics of turbulence are related to it by means of algebraic relations. Of these, most common are the models in which the equations of turbulent viscosity transfer are used, such as the Sekundov model and the Spalart–Allmaras model [3]. The former is used to calculate jets, mixing layers, and boundary layers, and the latter — to solve problems of subsonic aerodynamics and turbomachine building to calculate the boundary layers subjected to unfavorable pressure gradients [4].

The most representative group of differential models of turbulence consists of models with two equations (two-parametric ones or second-order ones). For near-wall flows, good results are obtained by using the k–ω model [5] and the k–ε model for the case of free shear layers [6]. The Menter shear stress transport (SST) model comprises the advantages of the above two models.

The application of the k–ε model is due to the difficulties in describing pressure-gradient boundary layers, swirled flows, laminar-turbulent transition, and compressible and separated flows (the model fails to satisfactorily predict the separation point). In order to take flow rotation into account, a modified form of representation of the turbulence production term [7] is used (the Kato–Launder correction), whereas the curvature of streamlines is accounted for by damping functions which depend on the turbulent Richardson number [2, 8].

Despite the well-known limitations, the everwidening use of the k–ε model in solving practical problems is attributable to the stable iteration process, the stability against the errors introduced with input data, and the reasonable accuracy for a wide class of turbulent flows. The k–ε model is practically included in all commercial computational packets intended for solving gas dynamics and heat-transfer problems (e.g., STAR-CD, CFX, and FLUENT).

In the k–ε model version developed on the basis of renormalization group (RNG) theory, the dissipation-rate equation is superposed by an additional condition, which improves the accuracy of solution for flows with high shear

D. F. Ustinov Baltic State Technical University "Voenmekh," 1 1st Krasnoarmeiskaya Str., St. Petersburg, 190005, Russia; email: dsci@mail.ru. Translated from Inzhenerno-Fizicheskii Zhurnal, Vol. 80, No. 1, pp. 90–99, January–February, 2007. Original article submitted July 4, 2005.

1062-0125/07/8001-0097

stresses. Here, the effect of turbulence circulation is also taken into account, thus increasing the accuracy of simulation of high-velocity rotational and circulatory flows. Unlike the standard model [6], an analytical dependence is introduced to calculate the turbulent Prandtl number in the process of solution.

In comparison with the model of [6], the realizable version of the k–ε model incorporates an improved method of calculation of turbulent viscosity, with the equation for the rate of dissipation being derived from an exact equation of transfer of the mean-square value of pulsation vorticity. This ensures a more accurate prediction of the characteristics of rotational flows, boundary layers subjected to strong pressure gradients, and separated and recirculatory flows, as well as the streams in which developed secondary flows exist.

From the viewpoint of computational resources, the Spalart–Allmaras model seems to be the most economical, since it uses one supplementary equation of transfer. The standard k–ε model needs a few more computational resources (two additional transfer equations to be solved). Because of the additional conditions and functions in the basic equations, as well as in connection with the higher nonlinearity, the realizable k–ε model requires more time for computation than the standard one.

The choice of the turbulence model exerts its influence not only on the expenditures of time on the iterative process but also on the convergence of numerical solution. In some cases, the standard k–ε model is a superdiffusional one, whereas its RNG version has been developed so that turbulent viscosity decreases on sharp changes in stresses. Since diffusion exerts a positive influence on the numerical solution convergence, the RNG model is more susceptible to solution instability in stationary problems.

The equations of the standard k–ε model in the formulation given in [6] are appropriate for describing only high-Reynolds flows (far from the wall). To find the flow parameters near the wall, the method of near-wall functions ($y^+ \approx 10$) is used. The striving to widen the limits of applicability of the k–ε model up to the wall has led to the creation of low-Reynolds versions, which are distinguished by the form of representation of the source terms in the equations of transfer of turbulence characteristics and by boundary conditions on the wall, as well as by damping functions [9]. The use of low-Reynolds models for calculation of three-dimensional flows seems to be rather expandable from the computational viewpoint, since the first node of the grid must be offset from the wall by a distance $y^+ << 1$. A compromise can be achieved by implementing a two-layer k–ε/k–l model, which presupposes division of the near-wall region into two subregions: in one of them (far from the wall), a high-Reynolds version of the model is realized, whereas in the other (close to the wall) — the one-parameter k–l model is realized. Here, it is necessary that $y^+ \approx 1$. It is recommended that approximately 10 nodes be present between the wall and $y^+ = 10$ and at least three nodes in the region of $y^+ < 5$.

The aim of the present work is to consider the characteristic features of the formulation of the two-layer model of turbulence and its use for calculating turbulent near-wall flows, elucidating the factors that exert their influence on the effectiveness of model realization and the means of widening the limits of its applicability, using, as an example, the calculation of a boundary layer on a flat plate with a longitudinal pressure gradient, to show the possibilities of the given model, and to compare the results of calculation of the heat-transfer characteristics obtained on the basis of the two-layer model, the k–ε model, and the Spalart–Allmaras model with the data of a physical experiment and available correlations.

Basic Equations. In the Cartesian coordinate system (x, y), an unsteady-state flow of a viscous compressible gas is described by the equation

$$\frac{\partial \mathbf{Q}}{\partial t} + \frac{\partial \mathbf{F}_x}{\partial x} + \frac{\partial \mathbf{F}_y}{\partial y} = 0 , \tag{1}$$

which is supplemented by the equation of state of a perfect gas:

$$p = (\gamma - 1)\,\rho \left[e - \frac{1}{2}\left(v_x^2 + v_y^2 \right) \right].$$

The vector of conservative variables $\mathbf{Q}$ and the vectors of fluxes $\mathbf{F}_x$ and $\mathbf{F}_y$ have the following form:

$$\mathbf{Q} = \begin{pmatrix} \rho \\ \rho v_x \\ \rho v_y \\ \rho e \end{pmatrix}, \quad \mathbf{F}_x = \begin{pmatrix} \rho v_x \\ \rho v_x v_x + p - \tau_{xx} \\ \rho v_x v_y - \tau_{xy} \\ (\rho e + p)\, v_x - v_x \tau_{xx} - v_y \tau_{xy} + q_x \end{pmatrix}, \quad \mathbf{F}_y = \begin{pmatrix} \rho v_y \\ \rho v_y v_x - \tau_{yx} \\ \rho v_y v_y + p - \tau_{yy} \\ (\rho e + p)\, v_y - v_x \tau_{yx} - v_y \tau_{yy} + q_y \end{pmatrix}.$$

The components of the tensor of viscous stresses and those of the heat flux vector can be found from the relations

$$\tau_{ij} = \mu_e \left(\frac{\partial v_i}{\partial x_j} + \frac{\partial v_j}{\partial x_i} - \frac{2}{3} \frac{\partial v_k}{\partial x_k} \delta_{ij} \right), \quad q_i = -\chi_e \frac{\partial T}{\partial x_i}.$$

The effective viscosity and thermal conductivity consist of a sum of molecular and turbulent coefficients of transfer:

$$\mu_e = \mu + \mu_t, \quad \chi_e = c_p \left(\frac{\mu}{\mathrm{Pr}} + \frac{\mu_t}{\mathrm{Pr}_t} \right).$$

To obtain molecular viscosity as a function of temperature the Sutherland law is used:

$$\frac{\mu}{\mu_*} = \left(\frac{T}{T_*} \right)^{3/2} \frac{T_* + B}{T + B},$$

where $\mu_* = 1.68 \cdot 10^{-5}$ kg/(m·sec), $T_* = 273$ K, and $B = 110.5$ K for air. The molecular thermal conductivity is related to the Prandtl number. The molecular and turbulent Prandtl numbers are assigned constant values (for air Pr = 0.72, $\mathrm{Pr}_t = 0.9$).

Turbulence Model. We will consider the characteristic features of formulation and implementation of the two-layer model of turbulence.

Outer and inner subregions. The near-wall region (boundary layer) is subdivided into two subregions — an inner and an outer one, with the boundary between them depending on the value of the local Reynolds number $\mathrm{Re}_y = \rho k^{1/2} y / \mu$, where y is the distance from the geometrical center of the control volume to the nearest wall. Usually it is assumed that $\mathrm{Re}_{y^*} = 150$–220 (with $y^+ = 100$–110).

In the outer high-Reynolds or entirely turbulent region (where $\mathrm{Re}_y > \mathrm{Re}_{y^*}$), the equations of the standard k–ε model [6] are used:

$$\frac{\partial k}{\partial t} + (\mathbf{v} \cdot \nabla)\, k = \nabla \left[\left(\nu + \frac{\nu_t}{\sigma_k} \right) \nabla k \right] + P - \varepsilon, \tag{2}$$

$$\frac{\partial \varepsilon}{\partial t} + (\mathbf{v} \cdot \nabla)\, \varepsilon = \nabla \left[\left(\nu + \frac{\nu_t}{\sigma_\varepsilon} \right) \nabla \varepsilon \right] + \frac{\varepsilon}{k} (c_{\varepsilon 1} P - c_{\varepsilon 2} \varepsilon). \tag{3}$$

The turbulent viscosity is calculated from the Kolmogorov–Prandtl formula:

$$\nu_t = c_\mu \frac{k^2}{\varepsilon}. \tag{4}$$

In the inner low-Reynolds or viscous region (where $\mathrm{Re}_y > \mathrm{Re}_{y^*}$), the one-parametric k–l turbulence model is used [10]. The kinetic energy of turbulence is determined from Eq. (2). In order to find the dissipation function, the solution of Eq. (3) is replaced by the relation $\varepsilon = k^{3/2} / l_\varepsilon$. The turbulent viscosity is calculated from the formula [11]

$$\nu_t = c_\mu l_\mu k^{1/2}. \tag{5}$$

Linear scales. The linear scales l_μ and l_ε are determined with the aid of the Prandtl mixing-path model with account for van Driest's correction. In a fully turbulent region, l_μ and l_ε change according to the linear law at a distance from the wall, whereas in a viscous sublayer their behavior deviates from the linear distribution.

Unlike the van Driest model, in which the velocity in the direction parallel to the wall is used as the characteristic velocity, in the two-layer model such a role is played by the quantity $k^{1/2}$ (for separated flows the situation in which the velocity vanishes is possible). The linear scales are proportional to the characteristic scale of turbulent vortices near the wall $l_y = \kappa y$, and they are determined from the relations [12, 13]

$$l_\mu = c_l y\left[1 - \exp\left(-\frac{\mathrm{Re}_y}{A_\mu}\right)\right], \quad l_\varepsilon = c_l y\left[1 - \exp\left(-\frac{\mathrm{Re}_y}{A_\varepsilon}\right)\right].$$

Here, A_μ = 50–70, $A_\varepsilon = 2c_l$, $c_l = \kappa c_\mu^{-3/4}$, and $\kappa = 0.42$. As a rule, the boundary between the subregions passes through the place where $l_\mu \sim 0.94 c_l y$ and viscous effects are negligibly small.

The versions of the two-layer turbulence model are distinguished by the scales l_μ and l_ε selected [12, 14]. In the model of [14], the quantity $\langle v_y'^2 \rangle^{1/2}$ rather than $k^{1/2}$ is used as the linear velocity scale, the latter quantity being the case in the model of [11, 12]. The turbulent viscosity is calculated by the formula [14]

$$\nu_t = \langle v_y'^2 \rangle^{1/2} l_\mu .$$

The dissipation function is determined from the relation

$$\varepsilon = \frac{\langle v_y'^2 \rangle^{1/2} k}{l_\varepsilon}.$$

The linear scales are calculated from the results of direct numerical simulation of a fully developed turbulent channel flow [14]:

$$l_\mu = 0.33y, \quad l_\varepsilon = \frac{1.3y}{1.0 + 2.12\nu/\left(\langle v_y'^2 \rangle^{1/2} y\right)}.$$

In order to find the standard value of velocity in the transverse direction, the following semiempirical relation is used:

$$\frac{\langle v_y'^2 \rangle^{1/2}}{k} = 4.65\cdot 10^{-5}\,\mathrm{Re}_y^2 + 4.00\cdot 10^{-4}\,\mathrm{Re}_y .$$

The subregions are butt-jointed at $\mathrm{Re}_{y^*} = 80$. The behavior of the damping functions used in different models is shown in Fig. 1.

Boundary conditions. As a boundary condition for the kinetic energy of turbulence on the wall the Neumann condition is used:

$$\frac{\partial k}{\partial n} = 0 .$$

Near the wall $l_\mu \approx \kappa y$; therefore, $\varepsilon = k^{3/2}/(\kappa y)$. There is no need for the dissipation function on the wall in the boundary condition. In the model of [15], we assume that on the wall

$$k = c_\mu^{-1/2} f u_* ,$$

where

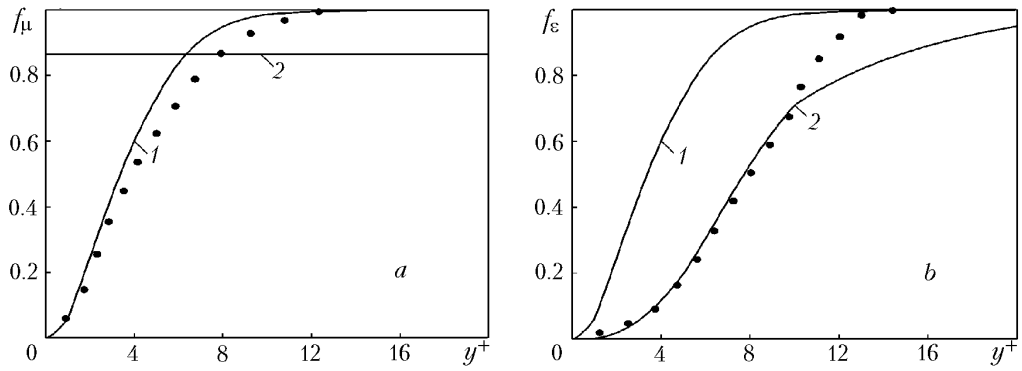

Fig. 1. Damping functions f_μ and f_ε for linear scales l_μ (a) and l_ε (b) used in the models of [11] (curve 1) and [14] (curve 2). Points correspond to the data of direct numerical simulation.

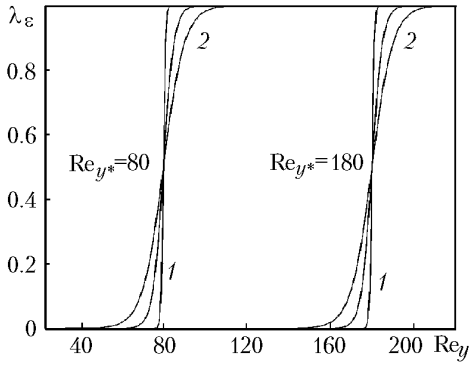

Fig. 2. Transition function at A = 1 (curves 1) and A = 10 (curves 2).

$$f = \begin{cases} 1, & y^+ \geq d^+; \\ (y^+/d^+)^2, & y^+ < d^+. \end{cases}$$

In practice, $8 \leq d^+ \leq 12$, and the above-indicated condition is imposed in the node closest to the wall.

Transition between the subregions. A sharp transition between the subregions leads to computational problems because of the divergence of the numerical solution. In order to ensure a smooth transition from one subregion to the other, a transition function λ_ε such that $\lambda_\varepsilon = 0$ near the wall and $\lambda_\varepsilon = 1$ far from it is used. The same approach is used in calculating the rate of dissipation, which allows one to guarantee a smooth transition between the solution obtained by solving Eq. (3) and the value found in the near-wall region.

In the simplest case, a linear transition is used. In particular, for the region in which $180 < \mathrm{Re}_y < 220$, the linear function of the transition has the form

$$\lambda_\varepsilon = \frac{220 - \mathrm{Re}_y}{40}.$$

In [16], it is suggested to use the following function:

$$\lambda_\varepsilon = \frac{1}{2}\left[1 + \tanh\left(\frac{\mathrm{Re}_y - \mathrm{Re}_{y^*}}{A}\right)\right].$$

The constant A allows one to control the smoothness of the transition from one model to another (Fig. 2), and it is determined so that the value of λ_ε could be equal to about 1% of the value far from the wall at the given range of

the local Reynolds number $\Delta \mathrm{Re}_y$; therefore $A = \Delta \mathrm{Re}_y/\tanh(0.98)$. Usually, in practice $\Delta \mathrm{Re}_y = (0.05–0.2)\mathrm{Re}_{y^*}$, in view of which $A = 1–10$ (here, the transition from one model to another occurs within the limits of several meshes of the computational grid).

The use of the transition function [16] makes it possible to avoid the explicit division of the computational domain into subregions. The function λ_k is introduced in addition to λ_ε. The equation for the kinetic energy of turbulence does not change (always $\lambda_k = 1$), whereas the equation for the dissipation function and the turbulent viscosity are multiplied by the function λ_ε. The turbulent viscosity is calculated from the interpolation formula

$$\nu_t = \lambda_\varepsilon \nu_{t1} + (1 - \lambda_\varepsilon)\, \nu_{t2} .$$

The source term in the equation of the dissipation-function transfer is replaced by

$$S_\varepsilon = \lambda_\varepsilon \left[\frac{\varepsilon}{k} (c_{\varepsilon 1} P - c_{\varepsilon 2} \varepsilon) \right] + (1 - \lambda_\varepsilon) \left[\alpha \left(\frac{k^{3/2}}{l_\varepsilon} - \varepsilon \right) \right].$$

Moreover, the convection and diffusion terms in the dissipation-function transfer equation are also multiplied by λ_ε. As a result, the equation for the dissipation function in the outer region of the flow has the form of Eq. (3), and in the inner region it is reduced to the following equation:

$$\frac{d\varepsilon}{dt} = -\alpha \left(\varepsilon - \frac{k^{3/2}}{l_\varepsilon} \right), \tag{6}$$

which has an exact solution:

$$\varepsilon\,(t) = \frac{k^{3/2}}{l_\varepsilon} - \varepsilon\,(0) \exp(-\alpha t) .$$

The constant $\alpha \approx 1$ controls the difference between ε and $k^{3/2}/\lambda_\varepsilon$.

Account for compressibility. In order to take into account the effects of compressibility, the following relations [17] are used:

$$l_\mu = c_l y \left(\frac{\rho_w}{\rho} \right)^{1/2} f_\mu\,(\mathrm{Re}_y) , \quad l_\varepsilon = c_l y \left(\frac{\rho_w}{\rho} \right)^{1/2} f_\varepsilon\,(\mathrm{Re}_y) .$$

As the velocity scale, the quantity $(\rho/\rho_w)^{1/2} k^{1/2}$ is introduced instead of $k^{1/2}$. The turbulent and local Reynolds numbers are calculated from the formulas

$$\mathrm{Re}_t = \left(\frac{\rho}{\rho_w} \right)^{1/2} \frac{k^2}{\nu_w \varepsilon} , \quad \mathrm{Re}_y = \left(\frac{\rho}{\rho_w} \right)^{1/2} \frac{k^{1/2} y}{\nu_w} .$$

Near the wall, $\mathrm{Re}_t = \kappa y^+ / c_\mu$ and $\mathrm{Re}_y = c_\mu^{-1/4} y^+$.

Results of Calculations. The possibilities of the two-layer model are demonstrated using as an example the calculation of a boundary layer on a flat plate with a longitudinal pressure gradient. Investigations of a turbulent boundary layer on the wall with a decrease or increase in pressure in the flow direction are of great practical value for calculating the resistance and heat transfer of an airplane wing or turbine blade, as well as the characteristics of flow in a diffuser [18].

G*eometry of a computational domain.* The geometrical model reproduces the conditions of flow in the interblade channel of a gas turbine. The characteristic distribution of pressure over the blade surface is shown in Fig. 3. A maximum pressure is observed in the frontal, leeward surface of the blade (section 1), where the flow is accelerated from subsonic to supersonic velocities. On the lower, suction side of the blade there is an inverse pressure gradient (section 2).

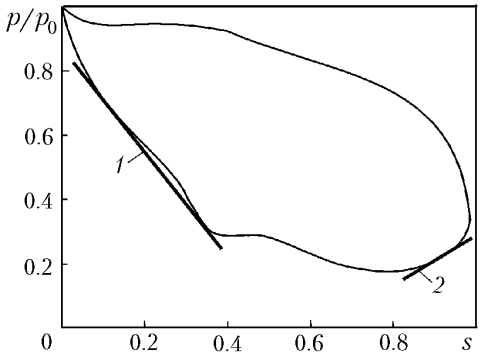

Fig. 3. Pressure distribution over the profiled body surface; sections 1 and 2 correspond to favorable and unfavorable pressure gradients.

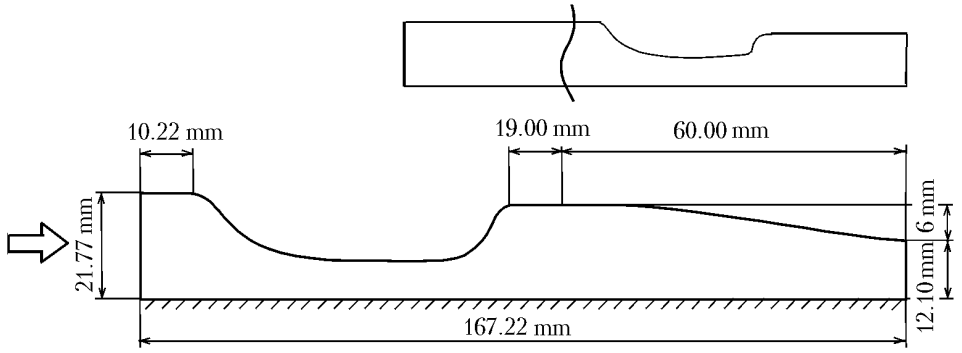

Fig. 4. Geometry of the computational domain.

We select the origin of the Cartesian coordinate system at the frontal point of the plate. The axis is directed along the plate (Fig. 4). The lower boundary of the computational domain is formed by the plate surface. The upper boundary consists of the linear segments and circular arcs and is constructed so that the pressure gradient created by the experimental setup [19] could be reproduced. Unlike that setup, the last section (where $x > 120$ mm) is made convergent to guarantee the convergence of the numerical solution. At the given values of the characteristic parameters of the problem, the flow in the exit section is supersonic; therefore, the features of the flow downstream of the indicated section do not exert any effect on the upstream parameters (the heat flux in the experiment in [19] was also recorded over that part of the plate surface where $x < 120$ mm).

The distribution of pressure along the plate surface, except for the small starting length, is virtually linear along the coordinate x (Fig. 5).

Initial and boundary conditions. It is assumed that at the initial moment the gas is at rest ($v_x = v_y = 0$, $p = 1.013 \cdot 10^5$ Pa, and $T = 288$ K). On the plate surface and upper wall, the boundary conditions of zero leakage and adhesion are imposed for the normal and tangential components of velocity, whereas the pressure is determined from the equation of change in the momentum resolved along the normal to the wall. The upper wall is considered to be insulated ($\partial T/\partial n = 0$). The plate surface has a constant temperature ($T = T_w$).

In the inlet section of the computational domain, the total pressure $p_0 = 3.66 \cdot 10^5$ Pa and stagnation temperature $T_0 = 280$–380 K are assigned and in the exit section — the static pressure $p = 1.013 \cdot 10^5$ Pa. In the calculations based on the k–ε model of turbulence, the kinetic energy of turbulence and the rate of its dissipation ($k_0 = 2$ m^2/sec^2, $\varepsilon_0 = 200$ m^2/sec^3) are assigned in the inlet section, whereas in the case where the Spalart–Allmaras model of turbulence was used, the assigned value was that of modified turbulent viscosity ($\tilde{\nu}_0 = 10^{-3}$ m^2/sec^2).

Numerical method. The discretization of the Navier–Stokes equations and that of a turbulence model is carried out with the aid of the control-volume method on a structured grid [20].

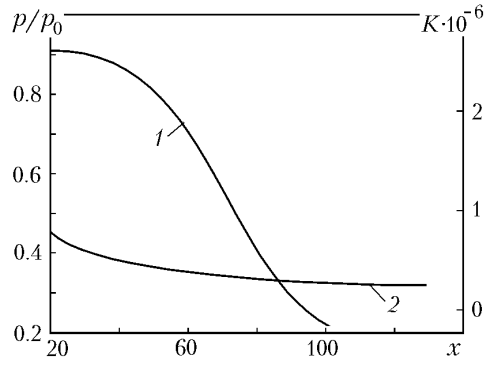

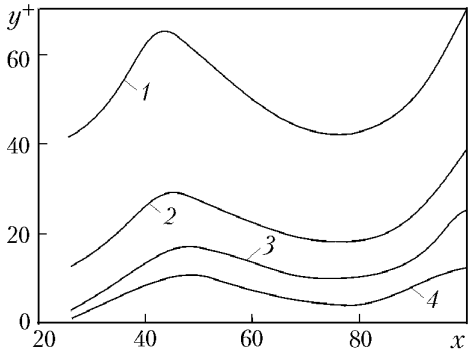

Fig. 5. Distributions of pressure (curve 1) and of the acceleration parameter (curve 2) along the plate surface. x, mm.

Fig. 6. Distributions of the quantity y^+ along the plate surface at 40 (1), 60 (2), 80 (3), and 100 (4) nodes in the transverse direction. x, mm.

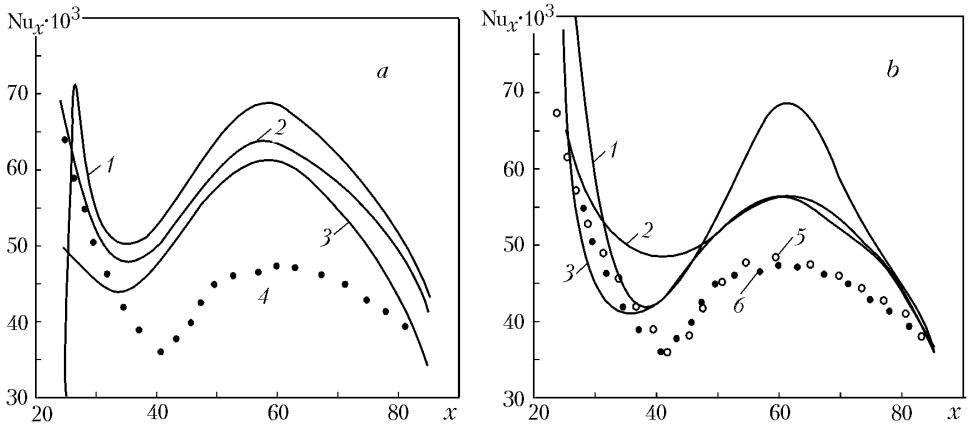

Fig. 7. Distributions of the local Nusselt number along the plate surface obtained on the basis of the Spalart–Allmaras model (a) and the k–ε model (b) at 40 (1), 60 (2), 80 (3), and 100 (4) nodes in the transverse direction; 5) results of calculation on the basis of the two-layer model of turbulence; 6) data of a physical experiment [19]. x, mm.

In order to perform discretization of time derivatives, the Runge–Kutta five-step method is used. The discretization of convective flows is carried out on the basis of the 3rd-order MUSCL scheme using the diagram of normalized variables [21] (a minmod is used). For the discretization of diffusion flows, 2nd-order centered difference formulas are used. The system of difference equations is solved by the multigrid method based on the scheme of complete approximation (four levels of a grid and V cycle are used).

Computational grid. In the calculations performed several grids are employed, which are characterized by different values of $y^+ = yu_\tau/\nu$, where $u_\tau = (\tau_w/\rho)^{1/2}$ is the dynamic viscosity, with τ_w being the surface friction stress. In the case of 40, 60, 80, and 100 nodes in the grid in the direction of the y axis, the grid contains 2870, 4140, 7614, and 14,500 meshes, respectively. The distributions of y^+ along the plate surface for grids of different resolving powers are shown in Fig. 6. Grids with 80 and 100 nodes across the flow have rather low values of y^+ near the plate surface, when the method of near-wall functions does not work [18].

Results of calculations. The local Nusselt number is determined from the relation

$$\mathrm{Nu}_x = \frac{qx}{\chi_\infty (T_\infty - T_w)} .$$

The distributions of the Nusselt number along the plate surface which were obtained on grids of different resolving power are shown in Fig. 7. With distance from the frontal edge of the plate the Nusselt number first decreases (with a minimum at $x \approx 38$ mm) and then again attains a maximum. It should be noted that at unfavorable and zero pressure gradients the dependences of the Nusselt number on the longitudinal coordinate are monotonically decreasing.

A favorable pressure gradient ($dp/dx < 0$) leads to a decrease in the heat fluxes directed to the plate surface as against the case of a nongradient flow [22, 23], exerting a rather strong influence on the velocity profile in the boundary layer and a comparatively slight influence on the temperature distribution [19]. At the same time, the measurements do not reveal a substantial influence of the inverse pressure gradient ($dp/dx > 0$) on the heat-transfer coefficient [18, 23].

On the whole, the k–ε model yields results which are about 10% better than those given by the Spalart–Allmaras model. However, admittedly the accuracy of the results obtained on the basis of these models is unsatisfactory. At the same time, the two-layer model of turbulence yields results which rather well agree with the data of a physical experiment [19], even through it requires an increase in the quality of the grid nodes across the flow (it is necessary that $y^+ \approx 1$, whereas for the method of near-wall functions $y^+ >> 1$) and about 20% less time for computation. The results of calculations by the two-layer model agree satisfactorily with the correlation given in [24].

Conclusions. The characteristic features of the formulation of a two-layer model of turbulence and its application to calculation of near-wall turbulent flows are considered. Factors exerting their influence on the effectiveness of the realization of the model are given, and ways of extending the limits of its applicability are discussed.

Numerical simulation of turbulent heat transfer of a flat plate in the presence of a longitudinal pressure gradient is carried out. The results of calculations show that the application of the standard k–ε model of turbulence and the Spalart–Allmaras turbulence model lead to unsatisfactory results, with the k–ε model giving results which are about 10–15% better. This is due to the insufficiently precise description of the flow structure in the boundary layer on the basis of the method of near-wall functions. In order to overcome the deficiencies indicated, a two-layer turbulence model is realized, which makes it possible to obtain estimates of the heat-transfer coefficient that are closer to the data of a physical experiment.

The results of calculations are of value for the investigation and control of the process of heat transfer of gas-turbine blades.

NOTATION

A, constant; B, constant in the Sutherland law, K; c_p, specific heat at constant pressure, J/(kg·K); c_l, c_μ, $c_{\varepsilon 1}$, and $c_{\varepsilon 2}$, constants of a turbulence model; d, distance to the wall, m; e, total energy of mass unit, J/kg; f, damping function; **F**, flow vector; k, kinetic energy of turbulence, m^2/sec^2; K, acceleration parameter; l, linear scale, m; n, normal; Nu, Nusselt number; p, pressure, Pa; P, turbulence generation term, m^2/sec^3; Pr, Prandtl number; q, heat-flux density, W/m^2; **Q**, vector of conservative variables; Re, Reynolds number; s, dimensionless coordinate reckoned along the surface of a profiled object; S, source term; t, time, sec; T, temperature, K; v_x, v_y, velocity components, m/sec; **v**, vector of velocity, m/sec; x, y, Cartesian coordinates, m; α, time constant, 1/sec; γ, ratio of specific heats; δ_{ij}, Kronecker symbol; ε, turbulent energy dissipation rate, m^2/sec^3; κ, von Karman constant; λ, transition function; μ, dynamic viscosity, kg/(m·sec); ν, kinematic viscosity, m^2/sec; ρ, density, kg/m^3; σ_k and σ_ε, constants in a turbulence model; τ, shear stress, N/m; χ, thermal conductivity, W/(m·K); ω, characteristic of a turbulence model, 1/sec; $\langle ... \rangle$, averaging in time. Subscripts; e, effective parameters of a turbulent flow; i, j, and k, tensor indices; t, parameters of a turbulent flow; x, y, projections to coordinate axes; w, wall; 0, stagnation parameters; 1, outer region; 2, inner region. Superscripts: *, critical parameters; +, dimensionless parameters in a boundary layer; ′, oscillations.

REFERENCES

1. E. P. A. Libby and F. A. Williams (Eds.), *Turbulent Reacting Flows*, Academic Press, New York (1994).
2. I. A. Belov and S. A. Isaev, *Modeling of Turbulent Flows* [in Russian], Izd. BGTU, St. Petersburg (2001).
3. P. R. Spalart and S. R. Allmaras, A one-equation turbulence model for aerodynamic flows, *AIAA Paper*, No. 92-0439 (1992).

4. S. Deck, P. Duveau, P. d'Espiney, and P. Guillen, Development and application of Spalart–Allmaras one-equation turbulence model to three-dimensional supersonic complex configurations, *Aerospace Sci. Technol.*, **6**, 171–183 (2002).
5. D. C. Wilcox, Dilatation–dissipation corrections for advanced turbulence models, *AIAA J.*, **30**, 2639–2646 (1992).
6. B. E. Launder and D. B. Spalding, The numerical computation of turbulent flows, *Comp. Meth. Appl. Mech. Eng.*, **3**, 269–289 (1974).
7. M. Kato and B. E. Launder, The modelling of turbulent flow around stationary and vibrating square cylinders, in: *Proc. 9th Symp. on Turbulent Shear Flows*, 16–18 August 1993, Kyoto, Japan (1993), Vol. 9, pp. 10.4.1–10.4.6.
8. M. A. Leschziner and W. Rodi, Calculation of annular and twin parallel jets using various discretization schemes and turbulent-model variations, *ASME J. Fluid Eng.*, **103**, 353–360 (1981).
9. J. Ch. Bonnin, T. Buchal, and W. Rodi, ERCOFTAC workshop on data bases and testing of calculation methods for turbulent flows, *ERCOFTAC Bulletin*, No. 28, 48–54 (1996).
10. M. Wolfshtein, The velocity and temperature distribution of one-dimensional flow with turbulence augmentation and pressure gradient, *Int. J. Heat Mass Transfer*, **12**, 301–318 (1969).
11. L. N. Norris and W. C. Reynolds, Turbulent channel flow with a moving wavy boundary, *Report of Stanford University*, No. FM-10 (1975).
12. W. Rodi, Experience with two-layer models combining the k–ε model with one-equation model near a wall, *AIAA Paper*, No. 91-0216 (1991).
13. H. C. Chen and V. C. Patel, Near-wall turbulence models for complex flows including separation, *AIAA J.*, **26**, No. 6, 641–648 (1988).
14. W. Rodi, N. N. Mansour, and V. Michelassi, One-equation near-wall turbulence modeling with the aid of direct simulation data, *J. Fluids Eng.*, **115**, 196–205 (1993).
15. M. Jaeger and G. Dhatt, An extended k–ε finite element model, *Int. J. Num. Meth. Fluids*, **14**, 1325–1345 (1992).
16. T. Jongen and Y. P. Marx, Design of an unconditionally stable, positive scheme for the k–ε and two-layer turbulence models, *Computers Fluids*, **26**, No. 5, 469–485 (1997).
17. D. Guezengar, J. Francescatto, H. Guillard, and J.-P. Dussauge, Variations on a k–ε turbulence model for supersonic boundary layer computations, *Eur. J. Mech. B/Fluids*, **18**, 713–738 (1999).
18. V. K. Garg, Heat transfer research on gas turbine airfoils at NASA GRC, *Int. J. Heat Fluid Flow*, **23**, 109–136 (2002).
19. A. J. H. Teekaram, C. J. P. Forth, and T. V. Jones, Film cooling in the presence of mainstream pressure gradients, *ASME J. Turbomachinery*, **113**, 484–492 (1991).
20. K. N. Volkov, Use of the control-volume method for solving problems of liquid and gas mechanics on unstructured grids, *Vychisl. Metody Programmir.*, **6**, No. 1, 43–60 (2005).
21. K. N. Volkov, Discretization of convective flows in the Navier–Stokes equations on the basis of high-resolution difference schemes, *Vychisl. Metody Programmir.*, **5**, No. 1, 129–145 (2004).
22. R. A. Seban and L. H. Back, Effectiveness and heat transfer for a turbulent boundary layer with tangential injection and variable freestream velocity, *ASME J. Heat Transfer*, **84**, 229–238 (1973).
23. H. Hay, D. Lampard, and C. L. Saluja, Effects of the condition of the approach boundary layer and of mainstream pressure gradient on the heat transfer coefficient on film-cooled surfaces, *ASME J. Eng. Gas Turbines Power*, **107**, 99–112 (1985).
24. W. M. Kays and M. E. Crawford, *Convective Heat and Mass Transfer*, McGraw-Hill, New York (1980).